Signatures of complex magnetic topologies from multiple reconnection sites induced by Kelvin-Helmholtz instability

Y. Vernisse, B. Lavraud, S. Eriksson, D. J. Gershman, J. C. Dorelli, C. Pollock, B. L. Giles, Nicolas Aunai, L. Avanov, J. L. Burch, et al.

HAL Id: hal-01551973
https://hal.science/hal-01551973

Submitted on 1 Nov 2021

Signatures of complex magnetic topologies from multiple reconnection sites induced by Kelvin-Helmholtz instability

Y. Vernisse[1,2], B. Lavraud[1,2], S. Eriksson[3], D. J. Gershman[4,5], J. Dorelli[4], C. Pollock[4], B. Giles[4], N. Aunai[6], L. Avanov[4,5], J. Burch[7], M. Chandler[8], V. Coffey[8], J. Dargent[1,6], R. E. Ergun[3], C. J. Farrugia[9], V. Génot[1,2], D. B. Graham[10], H. Hasegawa[11], C. Jacquey[1,2], I. Kacem[1,2], Y. Khotyaintsev[10], W. Li[10], W. Magnes[12], A. Marchaudon[1,2], T. Moore[4], W. Paterson[4], E. Penou[1,2], T. D. Phan[13], A. Retino[6], C. T. Russell[14], Y. Saito[11], J.-A. Sauvaud[1,2], R. Torbert[9], F. D. Wilder[3], and S. Yokota[11]

[1]Institut de Recherche en Astrophysique et Planétologie, Université Paul Sabatier, Toulouse, France, [2]Centre National de la Recherche Scientifique, Toulouse, France, [3]Laboratory for Atmospheric and Space Physics, University of Colorado Boulder, Boulder, Colorado, USA, [4]NASA Goddard Space Flight Center, Greenbelt, Maryland, USA, [5]Department of Astronomy, University of Maryland, College Park, Maryland, USA, [6]Laboratoire de Physique des Plasmas, Palaiseau, France, [7]Southwest Research Institute, San Antonio, Texas, USA, [8]NASA Marshall Space Flight Center, Huntsville, Alabama, USA, [9]Physics Department and Space Science Center, University of New Hampshire, Durham, New Hampshire, USA, [10]Swedish institute of Space Physics, Uppsala, Sweden, [11]Institute of Space and Astronautical Science, JAXA, Sagamihara, Japan, [12]Space Research Institute, Austrian Academy of Sciences, Graz, Austria, [13]Space Sciences Laboratory, Berkeley, California, USA, [14]Institute of Geophysics and Planetary Physics, and Department of Earth, Planetary, and Space Sciences, University of California, Los Angeles, California, USA

Abstract The Magnetospheric Multiscale mission has demonstrated the frequent presence of reconnection exhausts at thin current sheets within Kelvin-Helmholtz (KH) waves at the flank magnetopause. Motivated by these recent observations, we performed a statistical analysis of the boundary layers on the magnetosheath side of all KH current sheets on 8 September 2015. We show 86% consistency between the exhaust flows and particle leakage in the magnetosheath boundary layers but further highlight the very frequent presence of additional boundary layer signatures that do not come from the locally observed reconnection exhausts. These additional electron and ion boundary layers, of various durations and at various positions with respect to the leading and trailing boundaries of the KH waves, signal connections to reconnection sites at other locations. Based on the directionality and extent of these layers, we provide an interpretation whereby complex magnetic topologies can arise within KH waves from the combination of reconnection in the equatorial plane and at midlatitudes in the Southern and Northern Hemispheres, where additional reconnection sites are expected to be triggered by the three-dimensional field lines interweaving induced by the KH waves at the flanks (owing to differential flow and magnetic field shear with latitude). The present event demonstrates that the three-dimensional development of KH waves can induce plasma entry (through reconnection at both midlatitude and equatorial regions) already sunward of the terminator where the instability remains in its linear stage.

1. Introduction

Magnetic reconnection is a ubiquitous process in astrophysical plasmas with a particularly large impact in solar wind-magnetosphere interactions [*Cowley*, 1973]. The NASA Magnetospheric Multiscale (MMS) mission, launched on the 12 March 2015, aims to address many complex questions regarding the process of magnetic reconnection in the near-Earth environment by measuring plasma dynamics at the smallest scale: the electron scale [*Burch et al.*, 2015, 2016]. Magnetic reconnection may be triggered at various locations along the magnetopause. While it frequently occurs for relatively high magnetic shear angles between the reconnecting field lines, evidences of low shear magnetic reconnection has been investigated in various contexts [*Gosling et al.*, 2005; *Gosling and Phan*, 2013; *Hasegawa et al.*, 2004, 2009; *Nykyri et al.*, 2006].

During periods of northward interplanetary magnetic field (IMF), the Kelvin-Helmholtz instability occurs at the flanks of the Earth's magnetopause between the fast magnetosheath plasma and the slower magnetospheric plasma. This process has long been proposed to play an important role for momentum transfer at the magnetopause under such conditions [*Miura and Pritchett*, 1982, and references therein].

A second process has also been proposed for plasma transfer at the magnetopause under northward IMF. Solar wind and planetary field lines may reconnect at high latitudes at both ends and populate the low-latitude

boundary layer (LLBL) with solar wind plasma on newly closed dayside field lines [*Song and Russell*, 1992; *Sandholt et al.*, 1999]. This process increases the density in the LLBL in the equatorial plane. The occurrence of this process was later supported by observations, based on the use of heated electrons as tracers of magnetic topology [*Onsager et al.*, 2001; *Lavraud et al.*, 2005, 2006]. Magnetosheath electrons are heated when crossing the magnetopause. After entering the magnetosphere, they bounce at low altitude, closer to the ionosphere, and then escape back through the open magnetopause. They form a layer of escaping electrons with a higher temperature than the pristine, entering magnetosheath electrons (which have not yet crossed the magnetopause): the magnetosheath electron boundary layer [*Gosling et al.*, 1990]. The escaping electron directionality and layer width directly depend on the X line position relative to the spacecraft. Evidences for plasma transport through magnetic reconnection, diffusion, and other processes within nonlinear vortices have been reported [*Belmont and Chanteur*, 1989; *Nykyri et al.*, 2006; *Hasegawa et al.*, 2009; *Cowee et al.*, 2010; *Nakamura et al.*, 2011]. The KH instability develops mainly in the equatorial plane for strongly northward IMF, due to the stabilizing effect of magnetic tension at higher latitude [*Farrugia et al.*, 1998; *Foullon et al.*, 2008]. The main reconnection mechanisms induced by a KH instability, summarized in detail in the literature [*Nakamura et al.*, 2008, 2013], are Type I and Type II reconnection. The Type I mechanism occurs at the trailing edge of a KH wave, where the current sheet has been compressed by the instability, providing better conditions for low shear reconnection to occur. The type II mechanism occurs at the leading edge of well-developed KH vortices and is induced by the coalescence of the vortices. The differential velocities induced by KH waves and vortices between the magnetosheath and the magnetospheric plasmas generate a three-dimensional torsion of the field lines between the equatorial plane and higher latitudes at the flank magnetopause (Figures 2h and 2i). This mechanism has been proposed to trigger magnetic reconnection at midlatitudes, about 30,000 km away from the equatorial plane, in the Southern and Northern Hemispheres. Evidences for this mechanism were found in both 3-D simulations and observations [*Faganello et al.*, 2012, 2014; *Borgogno et al.*, 2015]. *Borgogno et al.* [2015] used tracers in a three-dimensional fluid simulation to identify field lines connected to midlatitude reconnection sites. The reconnected field lines are observed along the KH waves and vortices, just adjacent to the main current sheet, with an increasing number of connections as the instability grows. Although not mentioned at the time, we note that the mixing of ion populations on the magnetosheath side of the trailing edge of KH vortices, which was evinced in *Bavassano Cattaneo et al.* [2010] and *Nakai and Ueno* [2011], may be consistent with the occurrence of midlatitude reconnections.

Here we present statistical results of the boundary layers associated with local reconnection exhausts induced within KH waves, confirming and complementing the results by *Eriksson et al.* [2016] and *Li et al.* [2016]. We then focus on the possible signatures of concomitant north and south midlatitude reconnection in both electron and ion populations on the magnetosheath side of the trailing edge of the KH waves.

Assuming that the particle signatures are due to midlatitude reconnection, we explain how the combined occurrence of magnetic reconnection at these various locations produces highly complex magnetic topologies in the vicinity of KH waves, with several potential combinations of reconnection site locations. The observations are from the 8 September 2015, between 10:00 UT and 12:00 UT when the four MMS spacecraft encountered a long duration KH event at the dusk magnetospheric flank [*Eriksson et al.*, 2016]. Furthermore, since the KH waves remain in their linear stage, this event provides new insights to the role and type of plasma entry induced by the KH instability.

2. Instrumentation and Event Overview

We analyze data from the NASA MMS mission, whose primary objective is to study the electron scales of the magnetic reconnection. Therefore, an extremely high resolution set of instruments was developed [*Burch et al.*, 2015, 2016]. The particle measurements presented were recorded by the Fast Plasma Investigation [*Pollock et al.*, 2016], with a resolution of 30 millisecond (ms) for electrons and 150 ms for ions. We also utilize magnetic field measurements from the fluxgate magnetometers [*Russell et al.*, 2014], developed among the FIELD consortium [*Torbert et al.*, 2014]. The data presented are from MMS1, unless otherwise mentioned.

During this event, the MMS spacecraft were situated between 5.15 (at 9:30) and 4.73 (at 11:30) Earth radius (R_E) along the GSE x axis, $7.76\,R_E$ and $9.63\,R_E$ along the y axis, and $0.19\,R_E$ and $0.0319\,R_E$ along the z axis. Thus, the satellites were traveling along the duskside flank, close to the GSE equatorial plane, crossing the magnetopause from the magnetosphere side to the magnetosheath side.
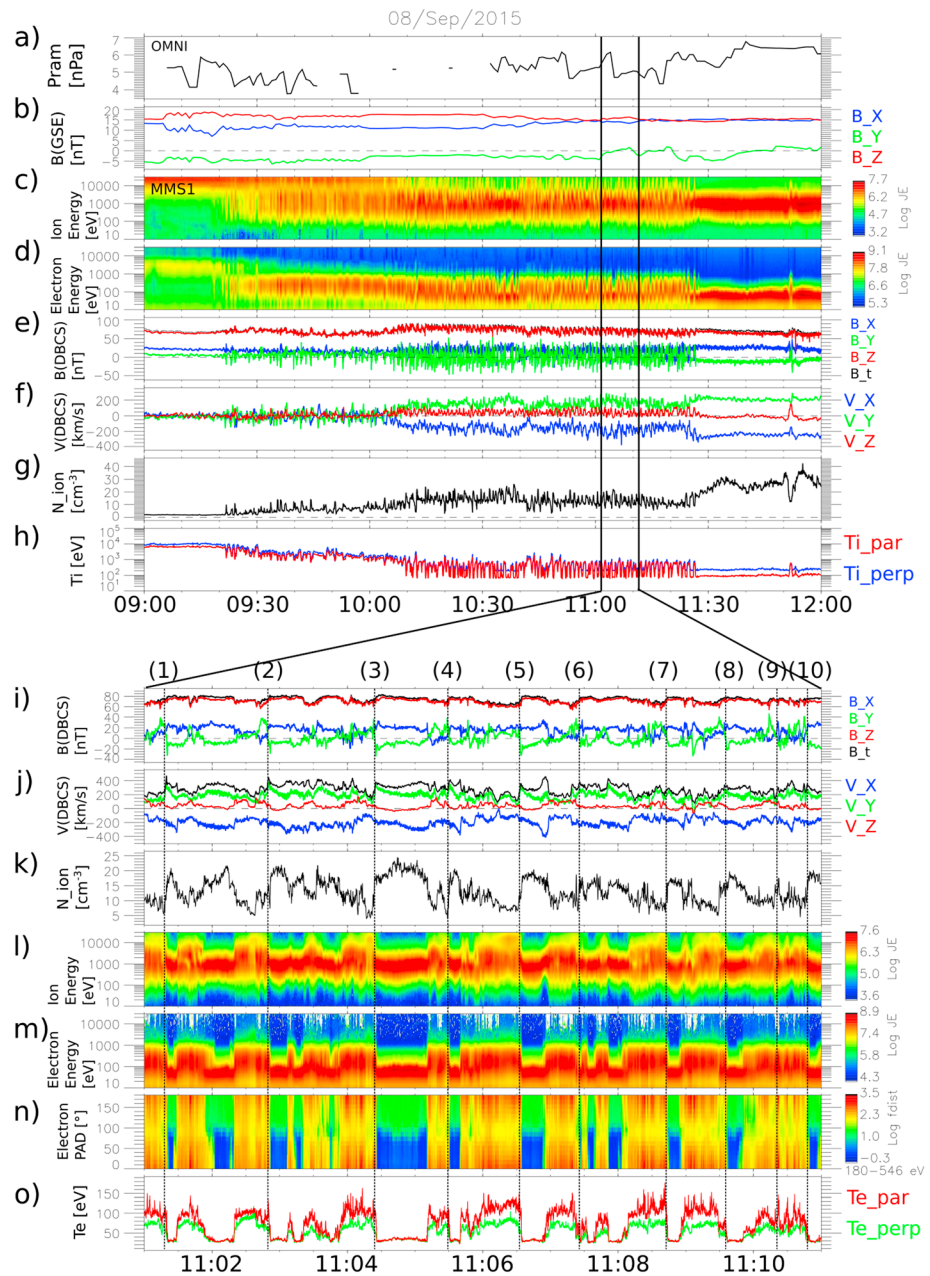
Figure 1. (a and b) OMNI ram pressure and magnetic field in GSE coordinate between 2015/09/08 at 09:00 and 2015/09/08 at 12:00. (c–h) MMS1 ion and electron energy spectrogram, magnetic field, ion bulk velocity, ion density, and ion parallel and perpendicular temperature, respectively, for the same time period. (i–o) MMS1 magnetic field, ion bulk velocity, ion density, ion and electron energy spectrogram, electron pitch angle distribution between 200 and 500 eV, and electron parallel and perpendicular temperature, respectively, for the time period between 2015/09/08 at 11:01 to 2015/09/08 at 11:11. Several current sheet crossings are identified with black dotted lines (see text).

Figure 1 presents an overview of the KH event and the associated context. The selected time period starts at 09:00 UT and ends at 12:00 UT (Figures 1a–1h). Figures 1a and 1b present the ram pressure and the magnetic field from OMNI data [*King and Papitashvili*, 2005]. OMNI data demonstrate that the solar wind parameters were very steady during the whole time period, with a dominant northward B_Z component consistent with the observation of KH instability. Figures 1c–1h show MMS1 ion and electron energy-time spectrogram, magnetic field, ion bulk velocity, ion number density, and ion temperature, respectively. The MMS spacecraft remain in the plasma sheet until 9:15, where they enter the low-latitude boundary layers. Shortly after, at 9:30,

successions of magnetopause crossings are observed, as shown by the multiple current sheet signatures in the MMS magnetic field measurements, best seen in the reversal in the B_Y component (Figure 1e). Typical signatures of the KH instability are observed from 09:30 UT to 11:25 UT, with a magnetopause crossing periodicity of ~30 s (see also *Eriksson et al.* [2016] and *Li et al.* [2016]). The MMS spacecraft finally exit into the magnetosheath proper at 11:30. A zoomed interval (between 11:01 and 11:11) is displayed in Figures 1i–1o. Figures 1i–1o display the magnetic field, ion bulk velocity, ion density, ion and electron energy spectrograms, electron pitch angle distributions (averaged on the energy range from 200 to 500 eV), and electron temperature, respectively. Several current sheet crossings (full and partial magnetopause crossings, from the magnetosphere to the magnetosheath) are distinguishable in the magnetic field measurement at (1) 11:01:20, (2) 11:02:50, (3) 11:04:20, (4) 11:05:30, (5)11:06:30, (6) 11:07:25, (7) 11:08:42, (8) 11:09:30, (9) 11:10:20, and (10) 11:10:40. Those current sheets have been indexed by *Eriksson et al.* [2016]. Most of the indexed crossings correspond to full outbound magnetopause crossings (from magnetosphere to magnetosheath). Those are typical crossings of the trailing (sunward facing) edge of a KH wave. Several current sheets correspond to partial outbound magnetopause crossings, i.e., the spacecraft does not exit into the magnetosheath proper. The variability of the sharpness of the magnetopause crossings is illustrated by the electron pitch angle distributions (Figure 1n). Strong bidirectional fluxes are observed inside the magnetopause at these energies, as typically found in boundary layer closed field lines inside the magnetopause [*Nishino et al.*, 2007]. Lower unidirectional fluxes are found at 180° pitch angle in the magnetosheath. This population corresponds to the strahl coming from the Sun. At small scales, magnetosheath electron boundary layers are observable, e.g., adjacent to crossing (1), on the outside of the current sheet. This is hardly observable in the present figure but will be further detailed in section 5. More complex features can also be seen, e.g., between crossing (9) and (10), where the spacecraft skims the magnetopause without fully crossing it. Inbound magnetopause crossings (from the magnetosheath to the magnetosphere) correspond to traversals of the leading (antisunward facing) edge of the KH wave. The leading edge, although steeper relative to the nominal magnetopause orientation [*Owen et al.*, 2004], is thicker than the trailing edge.

3. Model: Expected Topological Configurations

We show in the next sections the boundary layer signatures consistent with the probable occurrence of reconnection both locally in the equatorial region and at higher northern and southern latitudes. Before doing so, however, we list all possible scenarios that ensue from the proposed configurations. For each we explain the observational signatures which may be expected at a spacecraft located just outside the magnetopause current sheet within a vortex on its magnetosheath side. These are presented in Figures 2a–2d. Magnetic field lines are represented such that their magnetosheath parts are in red and their magnetospheric parts in blue. The three rectangles represent the regions where reconnection can occur—at midlatitude in the Southern and Northern Hemispheres and in the equatorial region, where the growth rate is deemed maximal. A dashed line within the rectangle means reconnection has occurred in that region, interconnecting magnetosheath and magnetosphere field lines. Regions were no reconnection has occurred are represented by a solid line within the rectangle.

Because the field lines can reconnect in three distinct regions—southern and northern midlatitudes, and at the local current sheet (Type I reconnection [*Nakamura et al.*, 2011])-—there are seven possible configurations. The Configurations 2, 4, and 5 are reversible by interchanging the two midlatitude regions (south or north) where reconnection may occur. In Figures 2b, e.g., the field line reconnects in the northern midlatitude region. A similar configuration is possible with a reconnection in the Southern Hemisphere and may be called 2bis. Similar reasoning applies to configurations 4 and 5 which may thus be called 4bis and 5bis later in the text (but not detailed).

1. Figure 2a: Pristine magnetosheath field line. There is no connection to any reconnection site, either locally or at higher latitudes. No heated electrons or ions (from connection to the magnetosphere through a reconnection site) are expected on this field line, neither field aligned nor anti-field aligned.
2. Figure 2b: One side of the magnetosheath field line is connected at one midlatitude reconnection site only, either south or north. In this case, parallel or antiparallel electrons are expected, depending on the hemisphere where the midlatitude reconnection site is located (in Figure 2b, antiparallel flowing electrons should be observed, as depicted in this figure for a reconnection site at northern midlatitude). Since the midlatitude reconnection point can typically be several tens of thousands kilometers away from
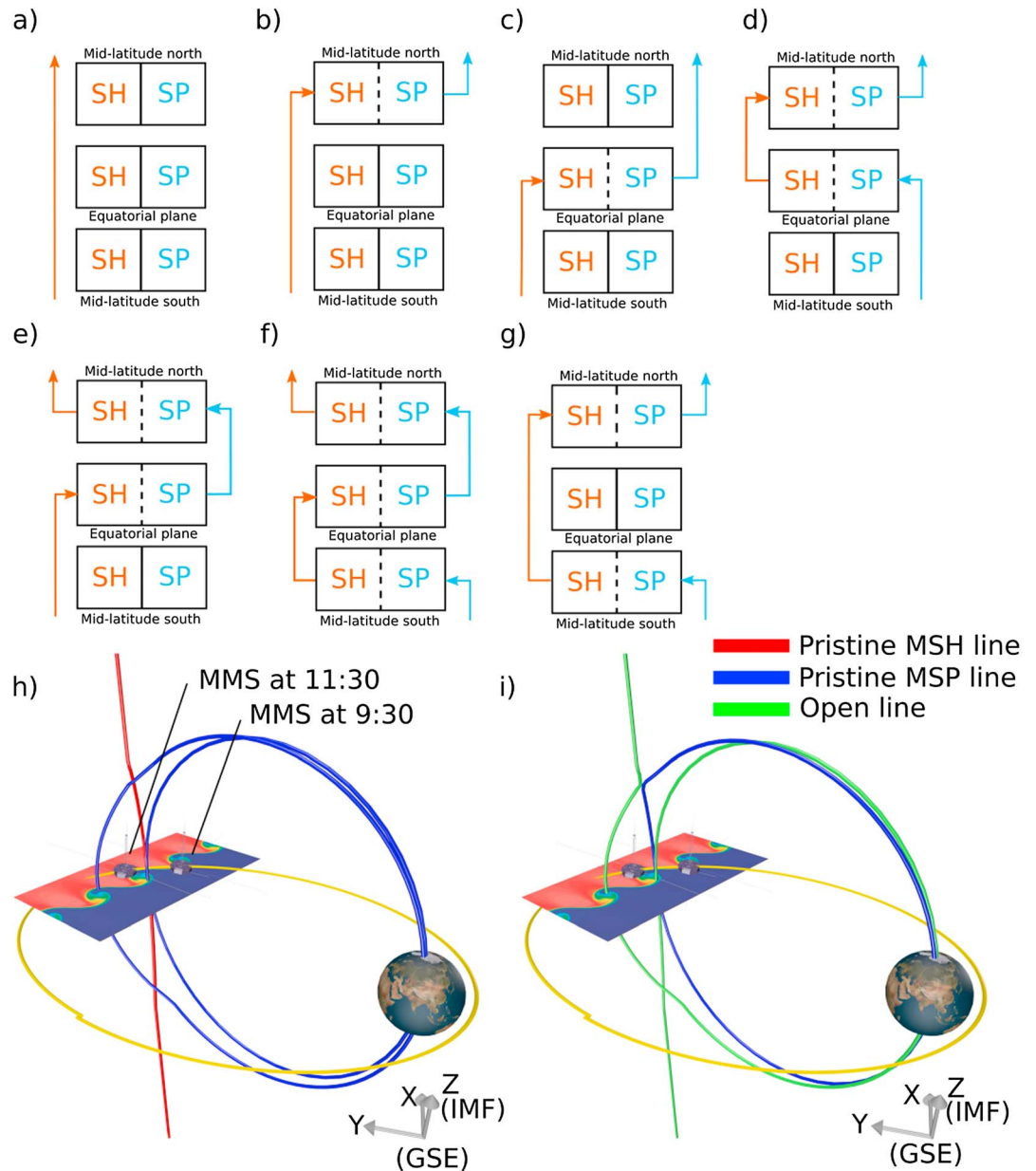
Figure 2. (a–g) Topologies of a field line observed on the magnetosheath side of a wavy magnetopause induced by the Kelvin-Helmholtz instability. SH corresponds to the magnetosheath side and SP to the magnetosphere side. A dashed line within the rectangle between the SH and SP parts means that reconnection is occurring at this particular site. A solid line within the rectangle signals that the magnetopause is closed at this site. (h and i) Example of field line changing topology. Two closed magnetospheric field line (blue) and one magnetosheath line (red) before (Figure 2h) and after (Figure 2i) reconnection have occurred in the local KH wave and at midlatitude north. The resulting open field line is depicted in green. The IMF is directed northward (+Z). The Sun is toward X.

the measurement point, at times one may expect the observation of parallel or antiparallel flowing ions coming from specular reflection at the reconnected magnetopause.

3. Figure 2c: One end of the field line is connected to the reconnection site triggered near the equatorial region of the KH wave. The magnetic field line is not connected to any other reconnection site. In this case one expects to observe a local exhaust with a small velocity jet (consistent with Walén relations) before exiting into the magnetosheath. In addition, a magnetosheath boundary layer with streaming heated magnetosheath electrons exiting the open current layer is expected. The heated electrons should be observed either parallel or antiparallel to the magnetic field, consistent with the local exhaust geometry

as detailed later. Owing to the proximity to the reconnection site (locally in the wave in the equatorial region), an observation of a magnetosheath boundary layer with specularly reflected ions is less likely (due to their much smaller velocities and ensuing boundary layer extent on the magnetosheath side of the exhaust).

4. Figure 2d: One end of the field line is connected at midlatitude in one hemisphere only, and the other end is connected to a local reconnection site in the KH wave. In this case, a local exhaust and associated short-duration magnetosheath electron boundary layer are expected (cf. configuration 3 above). But a population of heated streaming electrons is also expected in the other direction, coming from the more distant midlatitude reconnection site (cf. configuration 2 above). Owing to the farther distance to that reconnection site, streaming ions are conjectured as well, from that direction.

5. Figure 2e: In this configuration, the magnetosheath field line is not connected to any reconnection site on one end (here at its southern end) and extends into the solar wind. It is, at the other end, locally connected in the KH wave. The field line threading the local exhaust extends in the boundary layer on the magnetospheric side of the magnetopause, as for configuration 3, but in this case the field line is also reconnected at a more distant, midlatitude site from the inside of the magnetopause (here in the Northern Hemisphere). In such a case, an exhaust with a consistent unidirectional electron boundary layer should be observed locally, but no heated electrons are expected in the other direction (pristine magnetosheath electrons). Observationally, this configuration is unlikely to be differentiated from configuration 3, unless subtle differences in the amount of electron heating can be observed; i.e., because the (heated) electrons in the magnetosheath boundary layer have crossed the magnetopause at both midlatitude and the local reconnection site before observation at the spacecraft. It is merely listed here as an actual possible topology.

6. Figure 2f: This scenario is the most complex in that it involves reconnection of the same field line at three different reconnection sites. In addition to the connectivity of configuration 5 (one side connected to the local wave and a higher-latitude reconnection site in the same direction, i.e., the northern scenario in Figure 2e), the field line is additionally connected at the other end to another midlatitude reconnection site (here in the Southern Hemisphere). This topology can hardly be differentiated from configuration number 4 (same argument as for configuration 5). An exhaust with a consistent electron boundary layer should be observed in one direction. Streaming electrons and possibly ions are expected in the other direction (and likely over a broader interval owing to the more distant reconnection site), coming from the connectivity to a midlatitude reconnection site at the other end.

7. Figure 2g: The last configuration is that proposed by *Faganello et al.* [2012] and observed by *Faganello et al.* [2014]. It consists of a newly reconnected field line at both midlatitude locations. In this case, no local exhaust or short-duration magnetosheath electron boundary layer is expected, but longer duration heated electron (and possibly ion) populations are predicted both field-aligned and anti-field-aligned.

A summary of the seven possible configurations is provided in Table 1. In this table, we focus on describing for each case the connectivities of a field line observed by a spacecraft located in the equatorial region, on the magnetosheath side of the reconnection exhaust, between two trailing and leading current sheets of the developing Kelvin-Helmholtz wave. The two connectivities of the field line are described in the two column as connectivity 1 and connectivity 2, respectively. To each connectivity is attributed the particle signatures that are expected. If, e.g., a field line is connected on one end (connectivity 1) to a local reconnection exhaust, it implies observations of magnetospheric (MSP) electrons escaping either parallel or antiparallel (depending on which side of the X line the crossing occurs) along the field line. The same field line may for instance be connected at the other end (connectivity 2) to the pristine magnetosheath (MSH), and only magnetosheath electrons would be expected coming from that end. This case would be #3 in Table 1.

Figures 2h and 2i provide an artist view of a particular field line topology before and after reconnection has occurred, in this case locally at the equatorial and northern midlatitude regions. The MMS orbit on 08/09/2015 is represented in yellow, and the positions of the spacecraft at 9:30 (when entering the boundary layer) and 11:30 (when exiting in the magnetosheath) are shown. In Figure 2h, two magnetospheric field lines are plotted in blue. A magnetosheath field line is drawn in red. Figure 2i represents the same field line but after reconnection has occurred (1) in the wave in the equatorial region and (2) at northern midlatitude. This resulted in two open field lines, one directed from the southern magnetosheath toward the Earth's northern ionosphere, the other directed from the southern ionosphere toward the northern magnetosheath, and one

Table 1. Description of the Connectivities and Expected Particle Signatures on the Magnetosheath Side of a KH Wave as Observed by a Spacecraft Located in the Equatorial Region[a]

Cases	Connectivity 1	Connectivity 2
1	Pristine MSH	Pristine MSH
	MSH ion and electrons	MSH ions and electrons
2	Connected at one midlatitude site	Pristine MSH
	MSP electrons (possibly also ions)	MSH ions and electrons
3	Connected at local site	Pristine MSH
	MSP electrons (possibly also ions)	MSH ions and electrons
4	Connected at one midlatitude site	Connected at local site
	MSP electrons (possibly also ions)	**MSP** electrons (possibly also ions)
5	Connected at local site and one midlatitude site	Pristine MSH
	MSH heated 2 times electrons (possibly also ions)	MSH ions and electrons
6	Connected at local site and one midlatitude site	Connected at one midlatitude site
	MSH heated 2 times electrons (possibly also ions)	**MSP** electrons (possibly also ions)
7	Connected at one midlatitude site	Connected at one midlatitude site
	MSP electrons (possibly also ions)	**MSP** electrons (possibly also ions)

[a]The seven cases corresponds to the seven types of connectivities introduced in Figures 2a–2g. Connectivities 1 and 2 stand for the upper and lower ends of the observed field line, respectively, as depicted in Figure 2. Bold text denotes particles that are coming from one of the three identified reconnection sites possible: local within the wave and north and south midlatitude sites.

closed field line in blue. The green field lines correspond to configurations 3 (Figure 2c) and 2 (Figure 2b). The blue line corresponds to configuration 4 (Figure 2d).

4. Boundary Layer Identifications

To illustrate how we identify the various populations (in particular the magnetosheath electron boundary layer) coming from reconnection at various locations, we first introduce the particular geometry and signatures expected for reconnection induced at the trailing edge current sheet of the local wave in Figure 3.

The boundaries that we are mostly focusing on correspond to the trailing current sheet of the KH wave, where MMS moves from the magnetosphere to the magnetosheath. This crossing is the thinnest boundary in a KH wave [*Kivelson and Pu*, 1984]. At the boundary where the spacecraft goes from the magnetosheath to the magnetosphere, the plasma appears more turbulent and reconnection exhausts are harder to discern.

We use a similar coordinate system as in *Eriksson et al.* [2016], where N is the normal to the magnetopause, directed away from Earth. It is computed using the cross product of the mean value of the magnetic field vector on the magnetospheric side and on the magnetosheath side, around each crossing. A first maximum variance L_1 is computed from the Minimum Variance Analysis (MVA) [*Sonnerup and Scheible*, 1998] to build $M = N \times L_1$. The L direction completes the system so that LMN is a direct, orthogonal, and normalized coordinate system. In that system, the M direction is along the guide field, which is primarily northward (+Z GSE) and the L direction is typically along the reconnecting component of the
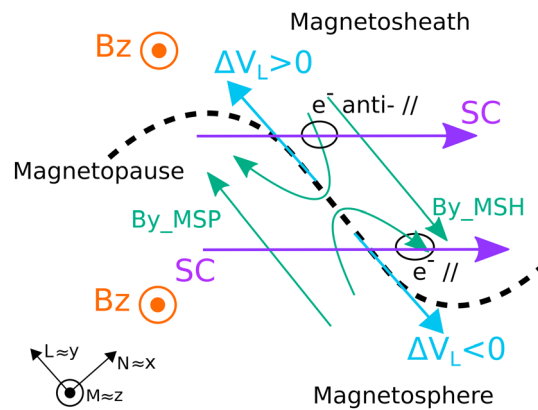
Figure 3. Structure at a reconnection site located between two Kelvin-Helmholtz waves. The IMF and magnetospheric field are mainly along +Z. By_MSP is the direction of the Y (GSE) component in the magnetosphere, and By_MSH is the direction of the Y component of the magnetic field in the magnetosheath. The GSE and LMN coordinate systems are mostly directed in opposite sense (see text). e⁻ anti // and e⁻ // stand for electrons antiparallel and parallel to the magnetic field, respectively, leaking out in the magnetosheath.. Whether e⁻ anti // or e⁻ // is observed depends on the crossing location of the spacecraft (earthward or anti-earthward of the X line), represented in purple.

exhaust, as shown in Figure 3 with a positive ΔV_L being directed anti-earthward. An LMN coordinate system is computed for each current sheet. In our systems, an earthward exhaust corresponds to a negative gradient of the ion velocity L component first, followed by a positive gradient. Overall, a negative excursion is observed in the L component of the ion velocity ($-\Delta V_L$). An anti-earthward exhaust similarly corresponds to a positive peak in L component of the ion velocity ($+\Delta V_L$). The LMN coordinate system of each current sheet is provided in the supporting information of *Eriksson et al.* [2016].

The schematic of Figure 3 presents the structure of the topology in the vicinity of an exhaust and of the magnetosheath electron boundary layer (EBL) associated and adjacent to it [e.g., *Gosling et al.*, 1990; *Lavraud et al.*, 2005]. An earthward directed exhaust ($-\Delta V_L$) means that the spacecraft is earthward of the X line. In that configuration, a boundary layer composed of hotter electrons (either initially hotter magnetospheric electrons or heated sheath electrons which have gone through the magnetopause one or several times) leaking out parallel to the magnetic field is expected to be measured by the spacecraft on the magnetosheath side. Similarly, next to an anti-earthward directed exhaust ($+\Delta V_L$), the EBL should be composed of heated electrons flowing antiparallel to the magnetic field. In either case, the layer of the heated streaming electrons should appear just adjacent to the exhaust and has a spatiotemporal extent commensurate with that of the exhaust.

5. Event Illustrations

We have selected four current sheets from *Eriksson et al.* [2016] for detailed analysis. We use them to illustrate identification of the EBL as well as the populations coming from midlatitude reconnection sites. The result of the analysis of the 42 current sheets reported in *Eriksson et al.* [2016], with the corresponding boundary layer properties—and links to local and midlatitude reconnection when the spacecraft is on the magnetosheath side—are provided in Table S1 of the supporting information.

Figures 4a–4d present a simple case of observation of a reconnection exhaust at the trailing edge of a KH wave on 8 September 2015. Details on the identification methodology such as Walén tests can be found in *Eriksson et al.* [2016]. Here we focus on the key signatures for our purposes: first, that of an EBL expected to be adjacent to the exhaust on the magnetosheath side. The data are presented in the LMN coordinate system, as explained earlier. The main rotation of the magnetic field (current sheet in Figure 4a) is observed in the L component, which is mainly along the Y GSE direction. The exhaust is observed in the ion velocity (Figure 4b), between 11:08:38.2 and 11:08:44, with a negative ΔV_L peak (with $\Delta V_L = -125$ km/s), therefore directed earthward. The ion velocity reasonably fulfills the Walén test on the two sides of the exhaust [cf. *Eriksson et al.*, 2016]. Figure 4c presents the electron pitch angle distribution (ePAD) for the energy range 230–546 eV. One can see bidirectional electrons in the magnetosphere, which is typical inside the magnetopause. Inside the exhaust (between 11:08:38.2 and 11:08:44), bidirectional electrons are present, with similar properties as in the preexisting boundary layer on the magnetospheric side of the exhaust. Just outside and adjacent to the exhaust, we observe a magnetosheath EBL between 11:08:44 and 11:08:45, with higher electron fluxes parallel to the magnetic field. The exhaust velocity being directed earthward ($-\Delta V_L$), the observation of parallel-flowing electrons in the boundary layer is thus consistent with a passage of the spacecraft earthward to the X line, as shown in the schematic of Figure 3. After this layer, predominantly antiparallel flowing electrons are observed with lower fluxes. These are the strahl electrons from the Sun [*Feldman et al.*, 1975]. The strahl electrons are easily identifiable in the whole data set. Their fluxes in the energy range between 200 and 500 eV are rather constant and much lower than the electrons leaking out from the magnetosphere by a factor of 10. Figure 4d shows the electron temperature parallel and perpendicular to the magnetic field. Higher temperatures are observed on the magnetospheric side, with a predominant parallel anisotropy as is often the case in low-latitude boundary layers on the flanks [e.g., *Nishino et al.*, 2007]. Enhanced temperatures are observed inside the exhaust.

Figures 4e–4h show data in the same format for a second exhaust event. This exhaust is chosen because this time the spacecraft crosses the magnetopause anti-earthward of the X line, consistent with the $+\Delta V_L$ peak inside the exhaust (with $\Delta V_L = +200$ km/s), between 10:47:06.5 and 10:47:09.6. The EBL (Figure 4g, between 10:47:09.6 and 10:47:10.7) adjacent to the exhaust is composed of heated electrons flowing antiparallel to the magnetic field, consistent with the schematic presented in Figure 3 in the case of a $+\Delta V_L$ exhaust flow. Of additional interest in the present case is the observation of heated electrons mainly in the antiparallel direction inside the exhaust, like in the magnetosheath EBL. This is unlike the first event where bidirectional
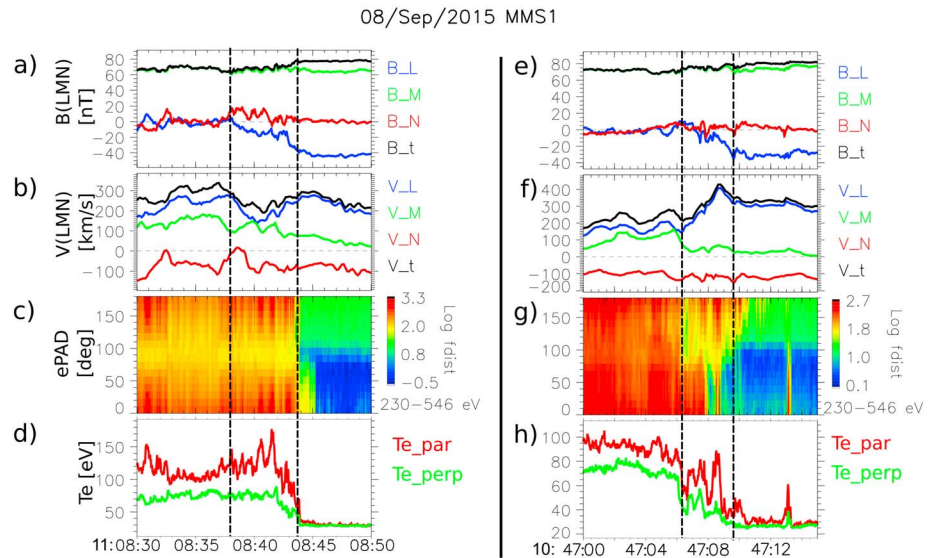
Figure 4. Two current sheets crossing on 8 September 2015 recorded by the MMS1 spacecraft, (a–d) between 11:08:30 and 11:08:50 and (e–h) between 10:47:00 and 10:47:25. Figures 4a and 4e and 4b, and 4f are the magnetic field and ion bulk velocity in LMN coordinates (see text), respectively. Figures 4c and 4g are the electrons pitch angle distribution for 250–500 eV, and Figures 4d and 4h are the electrons parallel (red) and perpendicular (geeen) temperatures.

heated electrons were observed throughout the exhaust. This suggests that in the present case the heating of inflowing electron does not only occur primarily at the outer exhaust boundary but also largely inside or at the inner exhaust boundary. These facts do not impact the main analysis presented here, but future investigations should address the question of main electron heating location. Those two events are noted as parallel and antiparallel, respectively, in the supporting information, consistent with the directionality of the exhaust velocity for each case in Figure 4. It should be noted that a second boundary layer was observed later during the magnetosheath traversals, outside of the intervals shown in Figure 4, for both events as noted in Table S1 columns 9 and 10. Figures 5a–5f now illustrate a more complex case. It displays the magnetic field and the velocity in LMN, the ePAD between 230 and 546 eV, the ion pitch angle distribution (iPAD) at 2 keV, and the electron and ion perpendicular and parallel temperature, respectively. The rotation of the magnetic field, as well as the exhaust, is observable between 10:20:58.2 and 10:20:59.8, with the ion exhaust velocity directed anti-earthward ($\Delta V_L = +100$ km/s). In Figure 5c, the EBL associated with the exhaust is observed adjacent to the end of the exhaust (white arrow). The escaping electrons are consistent with Figure 3, in the direction antiparallel to the magnetic field. Together with the antiparallel EBL, a population of heated electrons flowing parallel to the magnetic field is observed extending farther out in the magnetosheath (Figure 5c). This population is present throughout the magnetosheath interval in Figure 5c. It is not the strahl, which would have lower fluxes and be observed antiparallel to the magnetic field during this period. It should be noted that such an extended layer is not observed for every event, as can be noted in Figures 1 and 3 and in Table S1. Figure 5d shows the iPAD at 2 keV in the spacecraft frame. Hot magnetospheric ions with relatively isotropic iPAD are seen inside the magnetopause until 10:20:59.8. Throughout the exhaust (10:20:58.2 to 10:20:59.8) the iPAD is changing from nearly isotropic to perpendicular. Showing the iPAD in the spacecraft frame is in such a case useful to identify the magnetopause. Indeed, magnetosheath ions are much colder. Owing to the strong northward IMF and a largely tailward flow, they are characterized by a strongly peaked PAD at 90°.

A second event is presented in Figures 5g–5l. The structure is similar to that of Figures 5a–5f. The current sheet is observed between 10:44:32.5 and 10:44:34.5. *Eriksson et al.* [2016] reported a $-\Delta V_L$ exhaust (with $\Delta V_L = 80$ km/s) in this magnetopause (Figure 5h). The magnetosheath EBL is clearly observable in the ePAD (Figure 5i) between 10:44:34.5 and 10:44:40.2, with electrons flowing parallel to the magnetic field, again consistent with Figure 3. Heated electrons flowing both parallel and antiparallel to the magnetic field appear from 10:44:47.5 until the end of the time period, thus over an interval much more extended than for a mere EBL attached to an exhaust. Figure 5j shows the iPAD with typical signatures—perpendicular in the
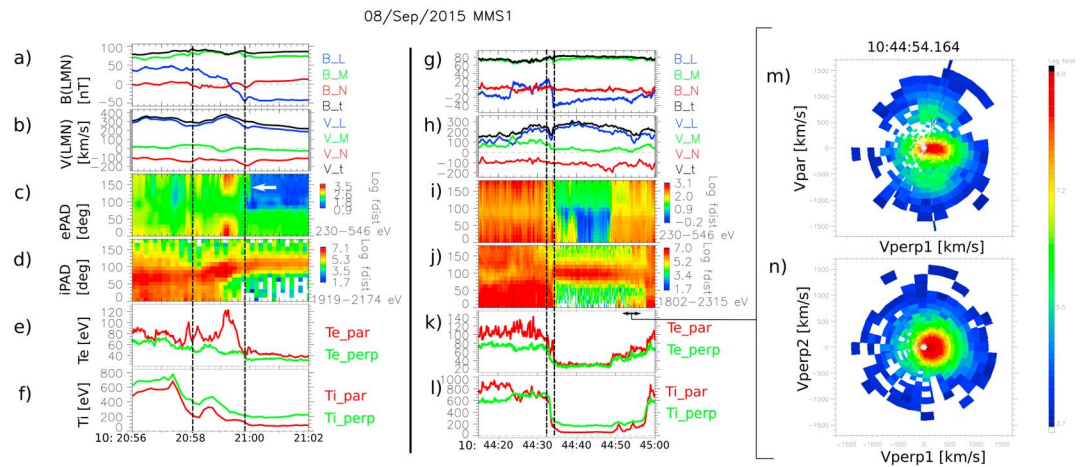
Figure 5. Data from the MMS1 spacecraft on 8 September 2015 (a–f) between 10:20:56 and 10:21:02, and (g–l) 10:44:18 and 10:45:00. The panels are similar as Figure 4 except that we added the (Figures 5d and 5j) ion pitch angle distribution (iPAD) at 2 keV, as well as the (Figures 5f and 5l) ion temperature. Figures 5m and 5n show the ion distribution averaged on the time period between 10:44:53.5 and 10:44:55.

magnetosheath and more isotropic in the magnetosphere—which suggest that the spacecraft is in the magnetosheath from 10:44:35.5 to 10:44:57.4. During this period, signatures of ions flowing parallel to the magnetic field are present from 10:44:50.5 to 10:44:57.4, and a strong signature of ions flowing antiparallel to the magnetic field is also observed between 10:44:54 and 10:44:56.6. Ion and electron temperatures (Figures 4k and 4l) are much lower than in the magnetosphere and thus consistent with these identifications.

Figures 5m and 5n show cuts of the ion velocity distribution function averaged between 10:44:53.5 and 10:44:55. Figure 5m is a cut in the V_{par}/V_{perp1} plane, while Figure 5n shows the cut in V_{perp2}/V_{perp1}. V_{par} is the component of the ion bulk velocity parallel to the magnetic field. V_{perp2} is directed along $B \times V$. V_{perp1} corresponds to convection direction and completes the right-handed coordinate system (V_{par}, V_{perp1}, and V_{perp2}). In Figure 5m, one identifies in red (largest phase space densities) the bulk velocity of the pristine magnetosheath ions, also present in Figure 5n. In addition, hotter parallel and antiparallel ions are noticeable in the distribution function (Figure 5m), within a range of 500 to 800 km/s along the magnetic field. These signatures suggest distant connection to an open magnetopause at both southern and northern latitudes, possibly like configuration 7 of Table 1 (corresponding to Figure 2g).

6. Discussion and Statistical Results

Figure 4 shows typical cases of reconnection occurring locally (relatively near the spacecraft) within KH waves close to the equatorial plane. *Eriksson et al.* [2016] estimated the normal width of the exhaust displayed in Figures 4a–4d to be about 67 km (using the ion bulk velocity projected onto the normal to the current sheet). Assuming that fast reconnection is occurring with a dimensionless reconnection rate of 0.1, the X line is estimated about 434 km away from the spacecraft. The size of the current sheet presented in Figures 4e–4h has a similar distance from the X line, with a width of 59 km and an X line distance of 304 km. This evaluation shows that MMS is located quite close to the reconnection site, and the observation of short-duration electron boundary layers associated with these exhausts just outside and adjacent to the outer current sheet is consistent with this interpretation. If reconnection only occurred locally in the wave, this configuration would correspond to type 3 in Table 1 and Figure 2c. The events presented in Figure 5, however, show multiple and more complex connectivities. As the spacecraft exits the exhaust in the first event (Figures 5a–5f), with an X line possibly situated 287 km away based on the exhaust size reported by *Eriksson et al.* [2016], MMS observes heated electrons leaking from the locally open current sheet, again consistent with the adjacent exhaust ion flow. But for this case the presence of a simultaneous and more extended layer of parallel heated electrons unambiguously signals a connection to another open magnetopause at the other end of the field line. Given the longer duration and directionality of this boundary layer, as opposed to the concomitant shorter boundary layer from the local exhaust, the heated electrons are interpreted as the signature of

connection to a reconnected magnetopause in the Southern Hemisphere at larger distances. This corresponds to configuration of Figure 2d (albeit with a south-north symmetry reversal), with the assumption that this other reconnection site is at high latitudes and associated with the large-scale entanglement owing to the wave.

The second event in Figures 5g–5l, with a local X line possibly 157 km away (again possessing a short electron boundary layer consistent with the local exhaust flow) also corresponds to a complex configuration with multiple topologies. Of specific interest in this event is the clear observation of both parallel and antiparallel flowing ions (observed as a 0° and 180° peaks in the ion PAD) which mix with the pristine magnetosheath ions (observed as a 90° peak in the ion PAD). The two ion populations are interpreted as specularly reflected ions at an open magnetopause, thus signaling the existence of reconnection sites at both southern and northern latitudes along the same field line (Figure 2g).

As the spacecraft is clearly located very close to the GSE equatorial plane (see Figure 2h) and records strong plasma periodicities associated with the passages of well-developed KH waves, it is reasonable to assume that MMS is located fairly central to the instability, rather than near the locations of high-latitude reconnection (as shown in Figure 2h). In other words, we can assume that the growth rate is close to its maximum near the spacecraft location. This assumption leads to the conclusion that the local jets studied here and in *Eriksson et al.* [2016] are Type I reconnection jets [*Nakamura et al.*, 2011]. Besides, the KH instability is identified to be in its linear stage [*Eriksson et al.*, 2016; *Li et al.*, 2016]. Thus, Type II reconnection jets, mainly observed in well-developed rolled-up vortices, are unlikely to be observed during the present event.

A statistical analysis of the magnetosheath boundary layers at the 42 current sheets observed by *Eriksson et al.* [2016] was performed, and details are provided in the supporting information Table S1. *Eriksson et al.* [2016] observed 22 exhausts using ion velocity signature. Four more exhausts were identified based on the electron velocity signature, and three more were noted as colliding jets.

From the 29 exhausts (including 4 exhausts identified with the electron velocity and 3 colliding jets [*Eriksson et al.*, 2013]) reported by *Eriksson et al.* [2016], 83% (24 events consisting of 8 and 12 ion exhausts with consistent antiparallel and parallel EBL, respectively, 3 antiparallel electron exhausts, and 1 colliding jet with a consistent EBL observed) showed leaking heated electrons outside the current sheet with the expected directionality (signaling leakage through the local boundary as depicted in Figure 3). Three cases showed a nonexpected directionality, and two cases are too unclear to conclude. Thus, the consistency between the direction of the exhaust velocity and the direction of the EBL according to the schematic of Figure 3 is fulfilled in 83% of the identified jets. In the remaining 13 current sheets where there is no evidence of a reconnection exhaust, 2 did not show a clear EBL adjacent to the current sheet. The other 11 cases, however, despite the absence of identified exhaust, presented a clear EBL, with 5 cases of electrons flowing parallel to the magnetic field and 6 cases of electrons flowing in antiparallel direction. Assuming that no local reconnection site was present in those 11 current sheets where no exhaust has been identified (although we acknowledge the lack of a clear local exhaust is likely not sufficient), one interpretation is that the heated electrons flowing in these boundary layers come from more distant sites, possibly from midlatitude reconnection sites. This statistic is provided in Table S2 of the supporting information.

A secondary statistics is provided in Table S1 (columns "MSH far electrons" and "MSH far ions") and summarized in Table S3. It focuses on the observations of more distant connectivity signatures found in the magnetosheath traversal interval as illustrated in Figure 5. Those signatures are electron and ion boundary layer not adjacent to the current sheets, in the interval where the spacecraft is in the magnetosheath. In 39 of the 42 events, the MMS1 spacecraft completely exits into the pristine magnetosheath, based on typical ion temperatures and pitch angle distribution as presented in Figure 5, and the traversal is sufficiently clear to deduce our results. Among those 39 magnetosheath traversal cases, 33 (85%) showed secondary (as introduced in Figure 5) EBL signatures during the magnetosheath traversal. We noted 20 cases of 39 magnetosheath traversal (51%) with bidirectional electrons and 13 cases (33%) with electrons flowing either parallel (12 cases) or antiparallel (1 case) to the magnetic field, thus possibly signaling southward and/or northward midlatitude reconnection sites (Figures 2b and 2g corresponding to types 2 and 7 of Table 1). For six crossings (15%), during the magnetosheath excursion all the way from the trailing edge to the leading edge of the KH waves—identified by a growing ion and electron temperature and isotropic ion and electron pitch angle distribution—MMS1 did not encounter any boundary layer signature of distant

reconnection (observed field lines are type 1 of Figure 2a and Table 1), as introduced earlier in the description of Figures 1e–1o. Magnetic field lines reconnected at a midlatitude site are observed adjacent to the current sheet and up to some distance from it [*Borgogno et al.*, 2015]. This is consistent with the various positions at which extended and intermittent electron boundary layer have been observed in the magnetosheath for the present event. Although the connectivity to distant reconnection sites at the leading edge of the observed KH waves is a fact, conclusions about the exact location of reconnection are difficult to draw owing to the particle signature only permitting to remotely sense the occurrence of reconnection.

In 20 cases of the 34 observations (59%) of distant EBL (as introduced in Figure 5), ion boundary layers in the magnetosheath were additionally observed. In 13 cases (38%), no ions were observed while electrons flowing either parallel, antiparallel, or both, to the magnetic field were identified far from the current sheet. More specifically, among the 20 reported bidirectional distant EBL, there were 9 consistently bidirectional (45%) distant ion boundary layer (IBL). Four cases showed antiparallel (20%) distant IBL, and four magnetosheath traversals had parallel (20%) IBL distant from the current sheet. This may be explained by the distance of the various reconnection sites from the observer; the ion boundary layer is known to have a spatial extent much smaller than that of electrons outside the magnetopause, owing to their much lower speeds. Besides, among the 12 parallel distant EBL, 3 cases had a consistently parallel distant IBL (25%), sustaining a type 2 topology (midlatitude connection only) field line (during the magnetosheath traversal) with connectivity to the Southern Hemisphere (Figure 2b). A summary of this statistics is provided in Table S3 of the supporting information.

The asymmetry between parallel and antiparallel particle signatures, with more events showing parallel-flowing particles in the boundary layers, may suggest that the field line encountered by the spacecraft are more often connected to a southern reconnection site. Further study on this possibility is left for future work.

Finally, since MMS is on the sunward side of the terminator, one could suggest that some of the magnetosheath electron boundary layers observed outside the magnetopause could be due to field lines connected poleward of the cusp through regular high-latitude reconnection under northward IMF [e.g., *Fuselier et al.*, 1997, 2012, 2014]. A permanent high-latitude reconnection is possibly identifiable in the V_Z component in Figure 1f, which shows periodic positive V_Z signatures in the magnetosphere side. However, while these ion flows may signal permanent higher-latitude reconnection, the EBL signatures on the magnetosheath side are clearly intermittent. For instance, our statistics show that there is often only one electron boundary layer consistent with local exhaust flows (as also observed from the larger perspective in Figures 1i–1o). The changing directionality of the electron boundary layer properties is rather consistent with more intermittent and complex reconnection processes occurring in the near vicinity of the waves, locally and at the tips of the waves in southern and northern midlatitudes, as depicted in Figure 3. This suggestion, however, deserves confirmation by future studies.

7. Conclusions

The numerous mechanisms taking place in association with the Kelvin-Helmholtz instability are still not fully uncovered. However, the unprecedented measurements provided by the MMS mission has already unveiled some of them. Direct signatures of reconnection at the trailing edges of the KH waves have been clearly identified [*Eriksson et al.*, 2016; *Li et al.*, 2016] together with midlatitude reconnection signatures. We have statistically confirmed that electrons leak out to the magnetosheath, consistent with the local exhaust properties (83%). Additional electron and ion populations are shown to be present in the magnetosheath, and those are suggested to come from midlatitude reconnection driven by the twisting of the field lines away from the KH waves in the Northern and Southern Hemispheres. This implies that multiple field line topologies can be encountered at the magnetopause during a KH event. It results in large-scale exchange and trapping of large bundles of plasmas in between the two midlatitude reconnection sites. To complete this study, we supply a statistics of 42 current sheets that MMS traversed, showing that the electron leaking out from midlatitude reconnection sites are observed almost 85% of the time. This suggests that this midlatitude reconnection mechanism could play a major role along with the Type I and Type II reconnection mechanisms earlier summarized by *Nakamura et al.* [2008]. Finally, this event demonstrates that the KH instability can lead to plasma entry induced by both equatorial (Type I) and midlatitude reconnections already on the dayside when the instability remains in its linear stage.

References

Bavassano Cattaneo, M. B., M. F. Marcucci, Y. V. Bogdanova, H. Rème, I. Dandouras, L. M. Kistler, and E. Lucek (2010), Global reconnection topology as inferred from plasma observations inside Kelvin-Helmholtz vortices, *Ann. Geophys.*, *28*, 893–906, doi:10.5194/angeo-28-893-2010.

Belmont, G., and G. Chanteur (1989), Advances in magnetopause Kelvin-Helmholtz instability studies, *Phys. Scr.*, *40*, 124–128, doi:10.1088/0031-8949/40/1/018.

Borgogno, D., Califano, F., Faganello, M., and Pegoraro, F. (2015), Double reconnected magnetic structures driven by Kelvin-Helmholtz vortices at the Earth's magnetosphere, *Phys. Plasmas*, *22*(3), 032301, doi:10.1063/1.4913578.

Burch, J. L., T. E. Moore, R. B. Torbert, and B. L. Giles (2015), Magnetospheric Multiscale overview and science objectives, *Space Sci. Rev.*, 1–17, doi:10.1007/s11214-015-0164-9.

Burch, J. L., et al. (2016), Electron-scale measurements of magnetic reconnection in space, *Science*, *352*(6290), doi:10.1126/science.aaf2939. [Available at http://science.sciencemag.org/content/early/2016/05/10/science.aaf2939.]

Cowee, M. M., D. Winske, and S. P. Gary (2010), Hybrid simulations of plasma transport by Kelvin-Helmholtz instability at the magnetopause: Density variations and magnetic shear, *J. Geophys. Res.*, *115*, A06214, doi:10.1029/2009JA015011.

Cowley, S. W. H. (1973), A qualitative study of the reconnection between the Earth's magnetic field and an interplanetary field of arbitrary orientation, *Radio Sci.*, *8*, 903–913, doi:10.1029/RS008i011p00903.

Eriksson, S., D. L. Newman, G. Lapenta, V. Angelopoulos, and M. V. Goldman (2013), Observations of colliding reconnection jets in the solar wind AGU Fall Meeting Abstracts.

Eriksson, S., et al. (2016), Magnetospheric Multiscale observations of magnetic reconnection associated with Kelvin-Helmholtz waves, *Geophys. Res. Lett.*, *43*, 5606–5615, doi:10.1002/2016GL068783.

Faganello, M., Califano, F., Pegoraro, F., Andreussi, T., and Benkadda, S. (2012), Magnetic reconnection and Kelvin-Helmholtz instabilities at the Earth's magnetopause, *Plasma Phys. Controlled Fusion*, *54*(12), 124037, doi:10.1088/0741-3335/54/12/124037.

Faganello, M., Califano, F., Pegoraro, F., and Retino, A. (2014), Kelvin-Helmholtz vortices and double mid-latitude reconnection at the Earth's magnetopause: Comparison between observations and simulations, *Europhys. Lett.*, *107*(1), 19001.

Farrugia, C. J., F. T. Gratton, L. Bender, H. K. Biernat, N. V. Erkaev, J. M. Quinn, R. B. Torbert, and V. Dennisenko (1998), Charts of joint Kelvin-Helmholtz and Rayleigh-Taylor instabilities at the dayside magnetopause for strongly northward interplanetary magnetic field, *J. Geophys. Res.*, *103*, 6703–6728, doi:10.1029/97JA03248.

Feldman, W. C., J. R. Asbridge, S. J. Bame, M. D. Montgomery, and S. P. Gary (1975), Solar wind electrons, *J. Geophys. Res.*, *80*, 4181–4196, doi:10.1029/JA080i031p04181.

Foullon, C., C. J. Farrugia, A. N. Fazakerley, C. J. Owen, F. T. Gratton, and R. B. Torbert (2008), Evolution of Kelvin-Helmholtz activity on the dusk flank magnetopause, *J. Geophys. Res.*, *113*, A11203, doi:10.1029/2008JA013175.

Fuselier, S. A., B. J. Anderson, and T. G. Onsager (1997), Electron and ion signatures of field line topology at the low-shear magnetopause, *J. Geophys. Res.*, *102*, 4847–4864, doi:10.1029/96JA03635.

Fuselier, S. A., K. J. Trattner, S. M. Petrinec, and B. Lavraud (2012), Dayside magnetic topology at the Earth's magnetopause for northward IMF, *J. Geophys. Res.*, *117*, A08235, doi:10.1029/2012JA017852.

Fuselier, S. A., S. M. Petrinec, K. J. Trattner, and B. Lavraud (2014), Magnetic field topology for northward IMF reconnection: Ion observations, *J. Geophys. Res. Space Physics*, *119*, 9051–9071, doi:10.1002/2014JA020351.

Gosling, J. T., and T. D. Phan (2013), Magnetic reconnection in the solar wind at current sheets associated with extremely small field shear angles, *Astrophys. J.*, *763*(2), L39, doi:10.1088/2041-8205/763/2/L39.

Gosling, J. T., M. F. Thomsen, S. J. Bame, T. G. Onsager, and C. T. Russell (1990), The electron edge of the low latitude boundary layer during accelerated flow events, *Geophys. Res. Lett.*, *17*, 1833–1836, doi:10.1029/GL017i011p01833.

Gosling, J. T., R. M. Skoug, D. J. McComas, and C. W. Smith (2005), Direct evidence for magnetic reconnection in the solar wind near 1 AU, *J. Geophys. Res.*, *110*, A01107, doi:10.1029/2004JA010809.

Hasegawa, H., M. Fujimoto, T.-D. Phan, H. Reme, A. Balogh, M. W. Dunlop, C. Hashimoto, and R. TanDokoro (2004), Transport of solar wind into Earth's magnetosphere through rolled-up Kelvin-Helmholtz vortices, *Nature*, *430*, 755–758, doi:10.1038/nature02799.

Hasegawa, H., et al. (2009), Kelvin-Helmholtz waves at the Earth's magnetopause: Multiscale development and associated reconnection, *J. Geophys. Res.*, *114*, A12207, doi:10.1029/2009JA014042.

King, J. H., and N. E. Papitashvili (2005), Solar wind spatial scales in and comparisons of hourly wind and ace plasma and magnetic field data, *J. Geophys. Res.*, *110*, A02104, doi:10.1029/2004JA010649.

Kivelson, M. G., and Z.-Y. Pu (1984), The Kelvin-Helmholtz instability on the magnetopause, *Planet. Space Sci.*, *32*, 1335–1341, doi:10.1016/0032-0633(84)90077-1.

Lavraud, B., M. F. Thomsen, M. G. G. T. Taylor, Y. L. Wang, T. D. Phan, S. J. Schwartz, R. C. Elphic, A. Fazakerley, H. Reme, and A. Balogh (2005), Characteristics of the magnetosheath electron boundary layer under northward interplanetary magnetic field: Implications for high latitude reconnection, *J. Geophys. Res.*, *110*, A06209, doi:10.1029/2004JA010808.

Lavraud, B., M. F. Thomsen, B. Lefebvre, S. J. Schwartz, K. Seki, T. D. Phan, Y. L. Wang, A. Fazakerley, H. Reme, and A. Balogh (2006), Evidence for newly closed magnetosheath field lines at the dayside magnetopause under northward IMF, *J. Geophys. Res.*, *111*, A05211, doi:10.1029/2005JA011266.

Li, W., et al. (2016), Kinetic evidence of magnetic reconnection due to Kelvin-Helmholtz waves, *Geophys. Res. Lett.*, *43*, 5635–5643, doi:10.1002/2016GL069192.

Miura, A., and P. L. Pritchett (1982), Nonlocal stability analysis of the MHD Kelvin-Helmholtz instability in a compressible plasma, *J. Geophys. Res.*, *87*, 7431–7444, doi:10.1029/JA087iA09p07431.

Nakai, H., and G. Ueno (2011), Plasma structures of Kelvin-Helmholtz billows at the duskside flank of the magnetotail, *J. Geophys. Res.*, *116*, A08212, doi:10.1029/2010JA016286.

Nakamura, T. K. M., M. Fujimoto, and A. Otto (2008), Structure of an MHD-scale Kelvin-Helmholtz vortex: Two-dimensional two-fluid simulations including finite electron inertial effects, *J. Geophys. Res.*, *113*, A09204, doi:10.1029/2007JA012803.

Nakamura, T. K. M., H. Hasegawa, I. Shinohara, and M. Fujimoto (2011), Evolution of an MHD-scale Kelvin-Helmholtz vortex accompanied by magnetic reconnection: Two-dimensional particle simulations, *J. Geophys. Res.*, *116*, A03227, doi:10.1029/2010JA016046.

Nakamura, T. K. M., W. Daughton, H. Karimabadi, and S. Eriksson (2013), Three-dimensional dynamics of vortex-induced reconnection and comparison with THEMIS observations, *J. Geophys. Res. Space Physics*, *118*, 5742–5757, doi:10.1002/jgra.50547.

Nishino, M. N., M. Fujimoto, T. Terasawa, G. Ueno, K. Maezawa, T. Mukai, and Y. Saito (2007), Geotail observations of temperature anisotropy of the two-component protons in the dusk plasma sheet, *Ann. Geophys.*, *25*, 769–777, doi:10.5194/angeo-25-769-2007.

Nykyri, K., A. Otto, B. Lavraud, C. Mouikis, L. M. Kistler, A. Balogh, and H. Reme (2006), Cluster observations of reconnection due to the Kelvin-Helmholtz instability at the dawnside magnetospheric flank, *Ann. Geophys.*, *24*, 2619–2643, doi:10.5194/angeo-24-2619-2006.

Onsager, T. G., J. D. Scudder, M. Lockwood, and C. T. Russell (2001), Reconnection at the high-latitude magnetopause during northward interplanetary magnetic field conditions, *J. Geophys. Res.*, *106*, 25,467–25,488, doi:10.1029/2000JA000444.

Owen, C., M. Taylor, I. Krauklis, A. Fazakerley, M. Dunlop, and J. Bosqued (2004), Cluster observations of surface waves on the dawn flank magnetopause, *Ann. Geophys.*, *22*, 971–983, doi:10.5194/angeo-22-971-2004.

Pollock, C., et al. (2016), Fast plasma investigation for Magnetospheric Multiscale, *Space Sci. Rev.*, *199*, 331–406, doi:10.1007/s11214-016-0245-4.

Russell, C. T., et al. (2014), The Magnetospheric Multiscale magnetometers, *Space Sci. Rev.*, *199*(1-4), 189–256, doi:10.1007/s11214-014-0057-3.

Sandholt, P. E., C. J. Farrugia, S. W. H. Cowley, W. F. Denig, M. Lester, J. Moen, and B. Lybekk (1999), Capture of magnetosheath plasma by the magnetosphere during northward IMF, *Geophys. Res. Lett.*, *26*, 2833–2836, doi:10.1029/1999GL900600.

Song, P., and C. T. Russell (1992), Model of the formation of the low-latitude boundary layer for strongly northward interplanetary magnetic field, *J. Geophys. Res.*, *97*, 1411–1420, doi:10.1029/91JA02377.

Sonnerup, B. U. Ö., and M. Scheible (1998), Minimum and maximum variance analysis, *ISSI Sci. Rep. Ser.*, *1*, 185–220.

Torbert, R. B., et al. (2014), The FIELDS instrument suite on MMS: Scientific objectives, measurements, and data products, *Space Sci. Rev.*, *199*(1-4), 105–135, doi:10.1007/s11214-014-0109-8.